# A Diagnostic System for Intracranial Saccular and Fusiform Aneurysms with Location Detection

Yousra Zafar and Ali Javed
*Department of Software Engineering*
*University of Engineering and Technology*
*Taxila, Pakistan*
yousrazafar2006@gmail.com,
ali.javed@uettaxila.edu.pk

Khalid Mahmood Malik, Jeremy Santamaria
*Department of Computer Science and Engineering*
*Oakland University*
*Rochester, MI 48309 USA*
mahmood@oakland.edu,
jfsantamaria@oakland.edu

Ghaus Malik
*Department of Neurosurgery,*
*Henry Ford Hospital,*
*Detroit, MI, USA*
gmalik1@hfhs.org

2021 IEEE EMBS International Conference on Biomedical and Health Informatics (BHI) | 978-1-6654-0358-0/21/$31.00 ©2021 IEEE | DOI: 10.1109/BHI50953.2021.9508536

**Abstract–Brain aneurysm detection is challenging due to multiple types of aneurysms, different image modalities, small size, and occurrence of aneurysms on multiple locations. Majority of brain aneurysm detection systems target only single class of aneurysm (i.e. saccular). Additionally, the detection of aneurysm location is largely unexplored. To overcome these challenges, we propose a robust two-stage brain aneurysm diagnostic system capable of detecting both forms of aneurysm (saccular and fusiform) along-with the detection of location. The first stage involves the aneurysm detection where vasculature extraction is performed initially using the morphological and enhancement operations. Next, histogram statistics are employed to obtain the potential aneurysmal region of interests (RoIs) that are later reduced using our proposed automated technique. We proposed a 28-D feature vector consisting of shape and texture features to represent these RoIs and used them to train a KNN classifier for aneurysm detection. The second stage focuses on the location detection where part of the vasculature with identified aneurysm is cropped and segmented via watershed segmentation. The distance of aneurysm to these segments is calculated and three smallest least distanced RoIs are identified. Next, we employed our 6-D shape features to represent these RoIs and fed to another KNN classifier for location detection. We achieved an accuracy of 95% for aneurysm detection and 82.6% for location detection on a dataset of 209 digital subtraction angiography (DSA) images acquired from the Henry Ford Hospital. These results signify the effectiveness of our system for aneurysm detection along-with its location identification.**

**Index Terms –Digital subtraction angiography, Cerebral Fusiform aneurysm, intracranial saccular aneurysm.**

## I. Introduction

Intracranial Aneurysms (IA), also termed as cerebral aneurysm, is a condition whereby a patient's blood vessels develop a balloon like outward swelling. This happens mainly due to the weakness in the walls of the blood vessels. When aneurysms become oversized, they tend to rupture because of increased blood pressure and cause the aneurysmal Subarachnoid Hemorrhage (aSAH), which represents a situation where blood flows into the cerebra of the patient causing serious damages like severe disability to spontaneous death. The two major shapes of IA are saccular and fusiform.

Automated aneurysm detection using neuroimaging modality is a challenging task because of the diverse equipment used, nature of angiogram technique, high intensity imaging, availability, appearance, and location of cerebral aneurysms. Existing computer aided detection techniques have employed various hand-crafted or deep learning-based features to develop the brain aneurysm diagnostic systems. In [1], Haralick features were used to train the multilayer perceptron classifier to detect the saccular aneurysms. Moreover, geometrical features were used to determine the risk of rupture. In [2], a semi-automatic deep learning-based approach was presented for aneurysm detection on 2D DSA images. This method requires manual processing of images for vessel extraction. In our prior work [3], an automated framework (ISADAQ) based on morphological, anatomical, and textural analysis was proposed to identify the saccular brain aneurysms on the DSA images. This framework also presented a semi-automated method for quantification of rupture prediction. This method is well suited for invasive DSA image modality only and efforts are required to extend this method on other image modalities. In [4], a system based on the creation of an ellipsoid convex enhancement (ECE) filter was presented to enhance the aneurysms from the images while suppressing the loops and overlays. In [5], authors focused on the enhancement of blob like areas from the images with the aim of detecting the small sized aneurysms from the vessels. The extensive research shows size of aneurysm alone is not a predictor of its rupture. For example [6-7] suggest that smaller aneurysms do also rupture resulting in aSAH. Findings of research work [6] concluded that 41% of the patients suffered aSAH with aneurysms as small as less than 5mm. The treatment decisions of intracranial aneurysm are not straightforward, and the risks of treatment have to be balanced cautiously against the risk of rupture [7]. However, the prediction of aneurysm rupture, based on combination of risk factors is a complex problem, and a reliable clinical computer-assisted tool for its diagnosis does not exist. However, there exist strong evidence that size ratio (IA size divided by parent vessel diameter), correlates strongly with IA rupture status [8]. Therefore, early identification of aneurysms along with its location (vessel)is crucial for to determine the probability of aneurysm rupture.

Most of existing computer aided image analysis works [1-5] have focused only on Saccular aneurysm detection without detecting its arterial location. Thus, to overcome the challenges of aneurysm of different type along with its location detection, we propose a robust brain aneurysm diagnostic system capable of effectively detecting the aneurysm of multiple types (i.e. saccular, fusiform) and location of aneurysm. According to the best of our knowledge, this is first attempt to detect both saccular and fusiform aneurysms along with their arterial location. For aneurysms detection of both types, we proposed a 28-D features-set

978-1-6654-0358-0/21/$31.00 ©2021 IEEE

consisting of shape and texture features (Table I) and used them to train the KNN for classification. Similarly, we proposed a 6-D shape features-set (Table I) and train the KNN for location detection. The main contributions of the proposed work are as follows:

TABLE I
FEATURES – SHAPE AND TEXTURAL

| Shape Features | Texture Features |
|---|---|
| Circularity | **GLCM** |
| Major Axis Length / Minor Axis Length | Contrast |
| Mean Intensity | Energy |
| Orientation | Homogeneity |
| Eccentricity | Correlation |
| EquivDiameter | **Haralick** |
| EulerNumber | Variance |
| Extent | Sum Average |
| **Location** | Sum Variance |
| Major Axis Length | Sum Entropy |
| Minor Axis Length | Entropy |
| Convex Area | Difference Variance |
| Area | Difference Entropy |
| Perimeter | Information Measure of Correlation I |
| Diameter | Information Measure of Correlation II |
| | MaximalCorrelationCoefficient |

- We propose an automated brain aneurysm detection system of both saccular and fusiform shapes based on the fusion of shape and texture features using DSA images.
- We present a novel brain aneurysm diagnostic framework capable of identifying both the aneurysmsand their cite/arterial location (e.g. Middle Cerebral Artery, Anterior Communicating Artery).

## II. METHODOLOGY

This section provides a discussion of the proposed method for detection of the aneurysm and its location. The block diagram of the proposed system is shown in Fig. 1.

### A. Aneurysm Detection

1) Pre-Processing and Vasculature Segmentation:Effective vasculature extraction is essential for accurate aneurysm detection. The presence of noise and other degradations make the vasculature segmentation a challenging task. Therefore, we applied various enhancement and morphological operators to improve the image quality before retrieving the vasculature from the image. The input colour image is transformed into a grayscale image. Next, histogram equalization is performed to enhance the image contrast. After contrast enhancement, image is upscaled by a factor of c=max/mean. Due to the presence of impulse noise, median filter is applied followed by the morphological closing operation to suppress the noise in the images shown in Fig.1.

Based upon the histogram counts of grey level values, the first six non-zero values are identified, and nine mask images are obtained based upon the individual and combination of these values. The details of these masks are as follows:

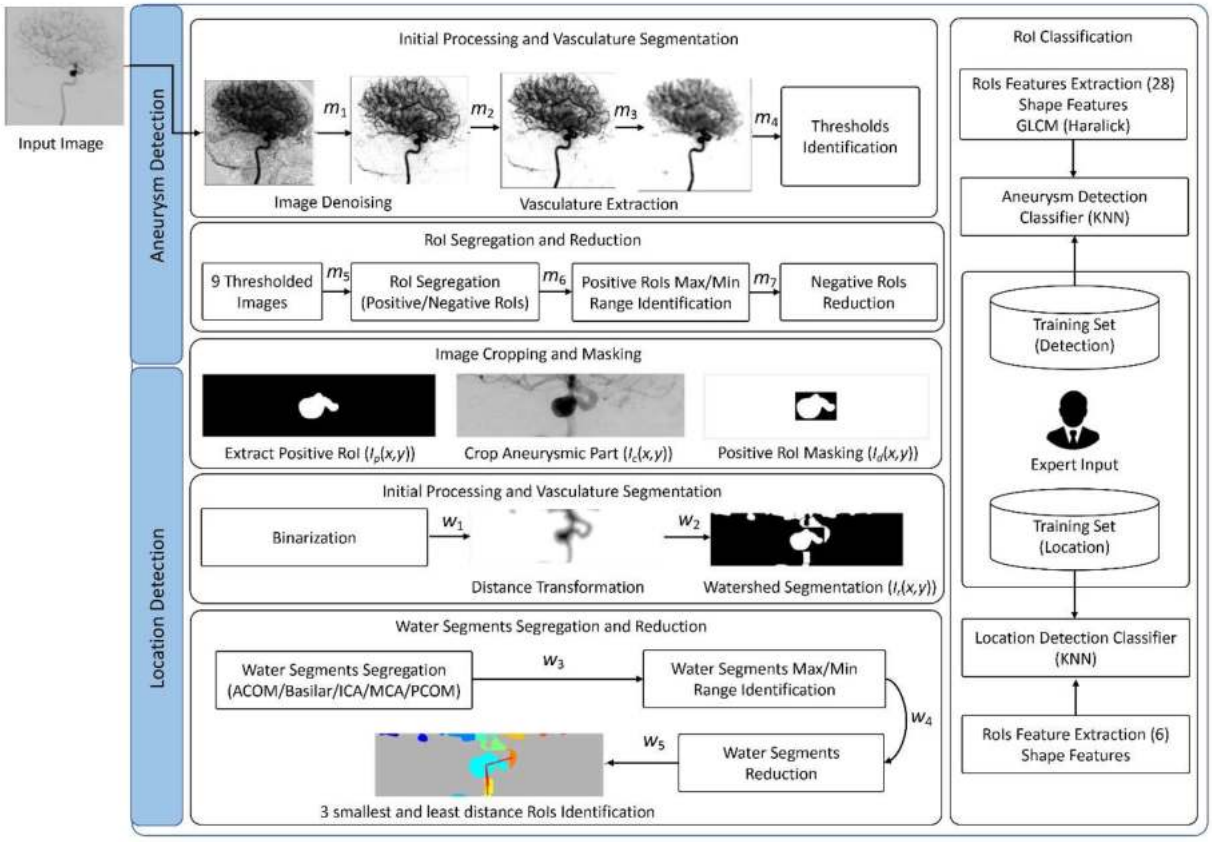


Fig. 1. Intracranial Saccular and Fusiform Aneurysm with Location Detection System

Mask 1: $I_b(x,y) > G_1$.
Mask 2: $I_b(x,y) > G_2$.
Mask 3: $I_b(x,y) >= G_2$ and $I_b(x,y) <= G_3$.
Mask 4: $I_b(x,y) >= G_3$ and $I_b(x,y) <= G_4$.
Mask 5: $I_b(x,y) >= G_4$ and $I_b(x,y) <= G_5$.
Mask 6: $I_b(x,y) >= G_5$ and $I_b(x,y) <= G_6$.
Mask 7: $I_b(x,y) >= G_2$ and $I_b(x,y) <= G_4$.
Mask 8: $I_b(x,y) >= G_3$ and $I_b(x,y) <= G_5$.
Mask 9: $I_b(x,y) >= G_4$ and $I_b(x,y) <= G_6$.
where $I_b(x,y)$ represents the black pixels in the image and $G_n$represents $n^{th}$ non zero grey level values.

2) Region of Interest (RoI) Segregation and Reduction: Nine masks' images are applied to the original images and only those regions are retained whose area >= 0.1. This helps in initial reduction of the negative RoIs (See Fig. 2). These RoIs are then manually segregated into positive and negative categories for the entire dataset. In our case, we obtained 297 positive RoIs and 39,225 negative RoIs from 209 DSA images of our dataset. We extracted our28-Dfeatures for positive RoIs and identified their min and max range. We retained those negative RoIs that lie within the range of positive RoIs that helped us to reduce the count of negative RoIs to 8,235.

3) RoIs Classification:We extracted the 28-D features from the negative and positive RoIs. To address the class imbalance issue, half of negative RoIs i.e 4086 is used against 297 positive RoIs. We employed our features to train a KNN for classification of aneurysm and non-aneurysm regions.

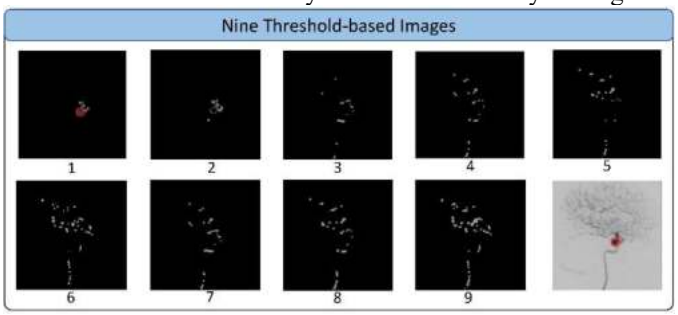


Fig. 2. RoI Segregation Using Nine Thresholds

B. Location Detection

1) Image Cropping, Masking and Segmentation: Location detection initially focuses on the identification of regional boundaries of aneurysm from the positive RoI image $I_p(x,y)$. Based upon these values, a horizontal rectangular cropping $I_c(x,y)$ of the vasculature is performed with aneurysm as the centroid. Later this rectangular cropped vasculature is up-scaled by a factor c=max/mean, de-noised via median filter, binarized, distance transformed and watershed segmented $I_w(x,y)$ based upon the location of water basins. There is a need to separate these water segments from the aneurysm. For this purpose, the resultant image $I_r(x,y)$is obtained by superimposing the positive RoI image cropped 5 pixels more than the actual width and height of the positive RoI $I_d(x,y)$ on $I_w(x,y)$.

2) Watershed Segments Segregation and Reduction: Initially all watershed segments are manually segregated to positive and negative RoIs. 6-D shape features for positive RoIs are extracted and their range in terms of max and min values is identified. The negative RoIs are reduced by retaining only those RoIs whose 6-D shape feature values lie within this range. Depending upon the centroid location of the positive aneurysm RoI, three smallest in terms of perimeter and least distanced RoIs are identified, as shown in Fig.1.

3) RoIs Features Extraction and Classification: A total of 334 positive RoIs are manually identified in a dataset of 171 images with positive aneurysm on 5 locations i.e Anterior Communicating Artery (ACOM), Basilar, Internal Carotid Artery (ICA),MCA, Posterior Communicating Artery (PCOM). A subset of 6-D shape features is extracted for these RoIs. We performed the up-sampling by using the vertical and horizontal flips (see Table II) to balance the count of each type of location RoIs. We employed our 6-D shape features to train the KNN for detecting the location of the aneurysm.

TABLE II
DETAILS OF UP-SAMPLING DATASET

| | Type | Old RoI Count | New RoI Count | Up-sampling Operation | | |
|---|---|---|---|---|---|---|
| | | | | OrigRoI | Hori Flip | Vert Flip |
| 1 | ACOM | 131 | 131 | ✓ | - | - |
| 2 | Basilar | 25 | 75 | ✓ | ✓ | ✓ |
| 3 | ICA | 45 | 135 | ✓ | ✓ | ✓ |
| 4 | MCA | 83 | 166 | ✓ | ✓ | - |
| 5 | PCOM | 50 | 150 | ✓ | ✓ | ✓ |

## III. EXPERIMENTS AND RESULTS

### A. Dataset

The availability of the dataset containing DSA images of both the saccular and fusiform brain aneurysm was a challenging task. We acquired 209 phase-contrast digital subtraction angiograms of patients from Henry Ford Hospital, Bloomfield Hills, MI, USA (IRB approval No. 11254). Patients' angiograms and other clinical data was anonymized before analysis. The data consisted of 158 angiograms with a single saccular aneurysm, 31 angiograms with a single fusiform aneurysm, and 20 angiograms without any aneurysm.

TABLE III
ANEURYSM DETECTION RESULTS ON FLIPPED ROIS

| | Type | Total +veRoIs | Total -veRoIs | True +ve Count | True –ve Count | Accuracy (%) |
|---|---|---|---|---|---|---|
| 1 | ACOM | 116 | 1757 | 115 | 1757 | 99.94661 |
| 2 | Basilar | 21 | 170 | 21 | 164 | 96.85864 |
| 3 | ICA | 27 | 451 | 27 | 451 | 100 |
| 4 | MCA | 68 | 772 | 68 | 772 | 100 |
| 5 | PCA | 18 | 115 | 18 | 115 | 100 |
| 6 | PCOM | 25 | 311 | 25 | 307 | 98.80952 |
| 7 | PICA | 10 | 61 | 7 | 57 | 90.14085 |
| 8 | Supraclinoid | 12 | 69 | 9 | 64 | 90.12346 |
| 9 | Fusiform-ACOM | 13 | 112 | 12 | 112 | 99.2 |
| 10 | Fusiform-MCA | 21 | 372 | 21 | 372 | 100 |
| 11 | Fusiform-PCA | 18 | 115 | 18 | 115 | 100 |
| 12 | Fusiform-PICA | 6 | 98 | 4 | 96 | 96.15385 |

### B. Performance Evaluation of Aneurysm Detection

For the aneurysm detection part, we segregated the overall RoIs into two categories i.e positive and negative RoIs. There

was a total of 297 positive RoIs and 39,217 negative RoIs. The negative RoIs were automatically reduced in a way that only RoIs lying within the max and min range of 28-D features of positive RoIs were retained. This helped in reducing the count of negative RoIs to 8,213. This count was still large, so half of these negative RoIsi.e.4,383 were randomly selected and used for training purpose. We extracted the features of both the positive and negative RoIs and fed to the classifier. We obtained an overall accuracy of 95%. It is also important to mention that we observed an improved classification accuracy when tested our model on the flipped positive RoIs. More specifically, we achieved an accuracy of 97.9% thus, achieved a performance gain of 2.9%. Table III shows the results when tested with flipped positive RoIs. From Table III, we can observe that we achieved optimal results (100%) on 3 locations of saccular aneurysm out of 8. Similarly, we achieved remarkable results on fusiform aneurysm on 2 locations out of 4. We observed a performance drop in saccular aneurysm detection for Posterior Inferior Cerebellar Artery (PICA) and Supraclinoid locations, and ACOM and PICA locations of fusiform aneurysm detection. This might be due to less aneurysm samples on those locations that reduces the accuracy of our system on these locations.

### C. Performance Evaluation of Aneurysm Location Detection

For the aneurysm location detection, a rectangular image containing the aneurysm at the center was cropped from the original image and later processed using the operations like binarization, distance transform and watershed segmentation. The obtained segments are automatically reduced based upon the max and min range of 6-D shape feature values of positive RoIs. Our system automatically identifies and classifies the three smallest RoIs in terms of perimeter and distance (least distanced RoIs) (See Fig.3).We achieved an overall accuracy of 82.6%. Table IV shows the results when tested with flipped positive RoIs. From the results, we can observe that we achieved 100% true positives (TP) rate on fusiform aneurysms, whereas, we also obtained 100% TP rate on 3 locations of the saccular aneurysm. On the MCA and PCOM arteries, we observed a slight performance drop due to some low-resolution images.

TABLE IV
RESULTS – ANEURYSM LOCATION DETECTION – FLIPPED ROIS

| | Type | RoI Count (Vert-Hori Flip) | Tue +ve Count | False – ve Count | %age True Positive |
|---|---|---|---|---|---|
| 1 | ACOM | 131 | 131 | 0 | 100% |
| 2 | Basilar | 25 | 25 | 0 | 100% |
| 3 | ICA | 45 | 45 | 0 | 100% |
| 4 | MCA | 83 | 81 | 2 | 97% |
| 5 | PCOM | 50 | 49 | 1 | 98% |
| 6 | Fusiform-ACOM | 7 | 7 | 0 | 100% |
| 7 | Fusiform-MCA | 27 | 27 | 0 | 100% |

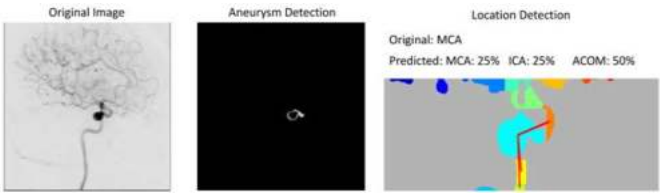


Fig.3. Final Results (a) Original Image (b) Detected Aneurysm (c) Detected Location

## IV. CONCLUSION

This paper has presented an automated brain aneurysm diagnostic framework capable of identifying both types of aneurysms i.e. Saccular and Fusiform along with the identification of 5 types of locations i.e ACOM, Basilar, ICA, MCA, PCOM, where aneurysm may be located. We employ various morphological and enhancement operations during preprocessing to reduce the noise and other degradations. Thus, improves the quality of input DSA image and makes our system capable of effective vascular extraction, which leads to effective aneurysm and location detection. For aneurysm detection, we employed 28-D (Shape and Textural) features-set to train a KNN classifier and obtained an accuracy of 95%. Moreover, we achieved a performance gain of 2.9% when tested our model on the flipped positive RoIs. More specifically, we obtained an accuracy of 97.9%. For location detection, we employed another KNN classifier trained upon 6-D shape features-set and attained 82.6% accuracy. We would like to highlight that the proposed system is the first attempt to develop an automated brain aneurysm diagnostic tool that is capable of not only detecting two classes of aneurysms but also the location of identified aneurysm. In the future, we plan to extend our system to support MRA and CTA image modalities, and also to improving the accuracy of our system.

## REFERENCES


[1] S. Anjum and K. M. Malik, “Saccular Brain Aneurysm Detection and Multi Classifier Rupture Prediction using Digital Subtraction and Magnetic Resonance Angiograms”, in CBBE '18: 5th International Conference on Biomedical and Bioinformatics Engineering, 2018.

[2] I. Rahmany, M. E. A.Nemmala, N. Khlifa, & H. Megdiche, “Automatic detection of intracranial aneurysm using LBP and Fourier descriptor in angiographic images”,International journal of computer assisted radiology and surgery, 14(8), 2019, 1353-1364

[3] K. M. Malik, S. M. Anjum, H.Soltanian-Zadeh, H. Malik, &G. M. Malik, “A framework for intracranial saccular aneurysm detection and quantification using morphological analysis of cerebral angiograms”, IEEE Access, 6, 2019, 7970-7986.

[4] H.Jin, J. Geng, Y. Yin, M. Hu, G. Yang, S. Xiang, &C. He, “Fully automated intracranial aneurysm detection and segmentation from digital subtraction angiography series using an end-to-end spatiotemporal deep neural network”, Journal of NeuroInterventional Surgery, 12(10), 2020, 1023-1027.

[5] T.Jerman, F. Pernuš, B. Likar, & Z. Špiclin, “Blob enhancement and visualization for improved intracranial aneurysm detection”, IEEE Transactions on Visualization and Computer Graphics, 22(6), 2015, 1705-1717.

[6] M. T. Bender, H. Wendt, T. Monarch, N. Beaty, L. M. Lin, J. Huang, & G. P. Colby,“Small aneurysms account for the majority and increasing percentage of aneurysmal subarachnoid hemorrhage: a 25-year, single institution study”, Neurosurgery, 83(4), 2018, 692-699.

[7] K. M. Malik, M. Krishnamurthy, F. Alam, H. M. Zakaria, G. M. Malik “Introducing the Rupture Criticality Index to Compare Risk Factors and Risk Factor Combinations Associated with Aneurysmal Rupture”, Journal of World Neurosurgery, 146, 2021, 38-47.

[8] Rahman, Maryam, Janel Smietana, Erik Hauck, Brian Hoh, Nick Hopkins, Adnan Siddiqui, Elad I. Levy, Hui Meng, and J. Mocco. "Size ratio correlates with intracranial aneurysm rupture status: a prospective study." Stroke 41, no. 5 (2010): 916-920.